Polarization-resolved critical-angle refractometry of liquid water (532–1551 nm, 25–80 °C)

Ierotheos Katsoulis · draft of Nov 4, 2026

Self-published preprint, not peer-reviewed. Text and figures © 2026 Ierotheos Katsoulis, licensed CC BY 4.0; analysis code MIT-licensed. Measurements were made at the Electronic Devices and Materials Laboratory (EDML), Department of Electrical and Electronic Engineering, University of West Attica, during an MSc by Research supervised by Prof. Konstantinos Moutzouris (2020–2021). The full measurement dataset may be the property of EDML, UNIWA and is not disclosed; a representative sample is provided for verification and is not covered by the CC BY license. *Cite as:* I. Katsoulis, "Polarization-resolved critical-angle refractometry of liquid water (532–1551 nm, 25–80 °C)," self-published preprint, November 2026.

Abstract

We find no optical anisotropy in liquid water at a glass-prism interface: after correcting a polarization-dependent bias of the derivative method, the difference between the refractive indices measured with TM and TE light is $(-0.04 \pm 0.91) \times 10^{-5}$, i.e. $|n_{TM} - n_{TE}| < 2 \times 10^{-5}$ at 95 % confidence.

We measured 252 critical-angle reflectance profiles of water with a prism-coupling refractometer at 532, 633, 964 and 1551 nm, in TE and TM polarization, between 25 and 80 °C. Taken at face value, the standard derivative method returns TM indices higher than TE by $(6.6 \pm 0.6) \times 10^{-5}$ — an apparent 11σ birefringence. A forward model of the reflectance edge, in which the Fresnel profile is blurred by the instrument's angular spread and then processed exactly like the data, reproduces the measured peak widths, edge reflectances and the TE/TM index difference without free parameters, showing that the apparent birefringence is a property of the analysis, not of water.

Two further systematic effects are identified and removed: an offset of $(9.3 \pm 1.8) \times 10^{-4}$ between scans taken with opposite table rotation, and a negative bias of 3.5–6.2 × 10^{-4} in all derivative-method indices. The corrected indices agree with the IAPWS R9-97 formulation, expressed relative to air, within the $\pm 1 \times 10^{-3}$ session-to-session reproducibility of the instrument, including at 1551 nm where the formulation is an extrapolation. At 633 nm the thermo-optic coefficient between 25 and 70 °C is $(-16.04 \pm 0.14) \times 10^{-5}$ K^{-1}, against -16.10×10^{-5} K^{-1} from IAPWS.

1. Introduction

Whether liquid water shows any optical anisotropy next to a solid surface is still open, and critical-angle refractometry can test it directly. Water near hydrophobic or hydrophilic surfaces orders over molecular to micrometre scales [5–11], and an ordered layer could make the refractive index depend on polarization. Earlier probes were mostly non-optical (NMR, conductivity) or spectroscopic, and one optical study of exclusion-zone water found no birefringence [9].

In critical-angle refractometry the sample is pressed against a prism of known index n_p and the reflectance $R(\theta)$ is recorded while the angle of incidence θ is scanned [1, 2]. The derivative method takes the critical angle θ_c as the maximum of $dR/d\theta$ and returns $n = n_p \sin \theta_c$ [16]. Because TE and TM are measured with the same prism and laser, most instrumental errors are common to both polarizations.

The catch is that the derivative maximum is not exactly the critical angle. Absorption [3, 17] and any finite angular resolution round the reflectance edge, and the rounding differs between TE and TM because their Fresnel coefficients approach total reflection differently. The extended derivative method of Koutsoumpos et al. [17] corrects the absorption part using the reflectance at the derivative maximum. This paper treats the instrumental part, which turns out to dominate for water.

We report TE and TM indices of water at four wavelengths (532–1551 nm) and up to 80 °C. The aims are (i) to bound $n_{TM} - n_{TE}$, (ii) to identify and remove the systematic errors that mimic anisotropy, and (iii) to compare the corrected indices and their temperature dependence with the IAPWS reference formulation [4, 12, 13].

2. Theory

For an isotropic sample the TE and TM reflectance edges sit at the same critical angle, but they have different shapes, so any process that shifts the derivative maximum shifts it by different amounts for the two polarizations.

2.1 Internal reflection at the prism–sample interface

Light in the prism (real index n_p) meets the sample (complex index $n = n_r + i\,k$) at internal angle θ. With the complex dielectric ratio $\varepsilon = (n/n_p)^2$ and $w = (\varepsilon - \sin^2\theta)^{1/2}$, taken with $\mathrm{Im}\, w \geq 0$, the Fresnel reflection coefficients are [17, 19]:

$$r_{\mathrm{TE}} = \frac{\cos\theta - w}{\cos\theta + w}, \qquad r_{\mathrm{TM}} = \frac{\varepsilon\cos\theta - w}{\varepsilon\cos\theta + w}, \qquad R = |r|^2$$

For a transparent sample ($k = 0$), $R = 1$ for $\theta \geq \theta_c$, where $\sin\theta_c = n/n_p$. Just below θ_c, $w \approx (\sin 2\theta_c \cdot \delta)^{1/2}$ with $\delta = \theta_c - \theta$, and

$$R_{\mathrm{TE}} \simeq 1 - \frac{4}{\cos\theta_c}\sqrt{\delta\,\sin 2\theta_c}, \qquad R_{\mathrm{TM}} \simeq 1 - \frac{4}{\varepsilon\cos\theta_c}\sqrt{\delta\,\sin 2\theta_c}$$

For water on a high-index prism $\varepsilon \approx 0.46$, so the TM edge drops about 2.2 times faster than the TE edge. Both derivatives diverge at θ_c, but the TE profile carries relatively more weight further below θ_c (Fig. 2).

2.2 Why the derivative maximum is biased

In practice the measured profile is the Fresnel profile convolved with the instrument's angular response: beam divergence, finite spot and detector aperture, plus the smoothing used to differentiate noisy data. Convolving a one-sided, square-root edge pulls the derivative maximum below θ_c, so the derivative method underestimates n. Because the TE edge has more weight away from θ_c, its maximum is pulled further than the TM maximum, and the analysis reports $n_{TM} > n_{TE}$ even for an isotropic sample.

Absorption acts the same way: with $k > 0$ the singularity at θ_c disappears, the edge rounds, and the maximum moves to a lower effective critical angle [3, 17]. The extended derivative method recovers n_r and k from the angle and reflectance at the maximum for a perfectly resolved profile [17]. For water at 532–964 nm, $k \leq 3 \times 10^{-6}$ [15, 18] and absorption is negligible; at 1551 nm, $k \approx 1.3 \times 10^{-4}$ and both mechanisms contribute.

We therefore model the recorded intensity as

$$I(\theta) = A\left[R_{\mathrm{pol}}(\,\cdot\,; n_r, k) * g_\sigma\right](\theta) + B$$

where g_σ is a normalized angular spread of standard deviation σ (Gaussian; a uniform kernel is used as a check) and A, B describe detector gain and offset. Passing simulated profiles through exactly the same code as the measured scans gives the bias $\Delta_{\mathrm{pol}}(\sigma, k) = n_{\mathrm{SDM}} - n_r$ for each polarization.

3. Experiment

All 252 scans were taken in six sessions on 30 October and 3 November 2020 with a Metricon 2010/M prism coupler [23] at the Electronic Devices and Materials Laboratory, University of West Attica (Fig. 1).

Instrument. A collimated, linearly polarized laser beam (≈ 0.8 mW) enters a high-index prism and reflects at its base. The prism and sample cell rotate together on a computer-controlled table, and a photodetector records the reflected intensity I as a function of the internal angle θ. TE or TM polarization is selected by a computer-controlled polarizer. The table steps 0.0075° externally, about 0.0036° internally, and each scan covers roughly 39–45° in 800–1500 points.

Prism index. The instrument converts angle to index with prism indices of 1.9775, 1.9642, 1.9450 and 1.9340 at 532, 633, 964 and 1551 nm (25 °C), quoted relative to air. It corrects them for prism temperature with dn_p/dT = 1.82, 1.69, 1.57 and 1.57 × 10^{-5} K^{-1}; for example n_p(532 nm) rises to 1.9785 at 80 °C. We use the instrument's temperature-corrected n_p for every scan. An earlier analysis of these data used the 25 °C value at all temperatures, which biases the 70 °C indices by about 6 × 10^{-4}.

Sample and temperature. A cell with an opening in its base was clamped to the prism, and water for injection was added with a syringe to avoid trapped air. The prism was held at 25, 50 (once 52), 70 or 80 °C, read with ±0.5 °C uncertainty. Before each polarization series the cell was emptied, refilled and re-clamped, and the table was auto-referenced for the laser in use. All TE scans of a condition were therefore taken on one filling and all TM scans on another.

Rotation direction. At 25 and 70 °C, consecutive scans alternate between the two directions of table rotation, labelled L and R. The 50 and 80 °C runs did not record the direction.

Session	Date (2020)	Time	λ (nm)	T (°C)	TE / TM scans	Direction
A	30 Oct	14:22–14:35	633; 532	50/52; 50, 80	2/1; 10/9	not recorded
B	30 Oct	17:43–18:37	532	25	19/19	L and R
C	30 Oct	19:30–20:14	633	70, then 25	28/28	L and R
D	30 Oct	20:35–20:58	532	70	9/9	L and R
E	3 Nov	13:18–14:59	964	25	30/28	L and R
F	3 Nov	15:16–16:06	1551	25	30/30	L and R

Table 1. Measurement sessions, reconstructed from the time stamps in the data files.

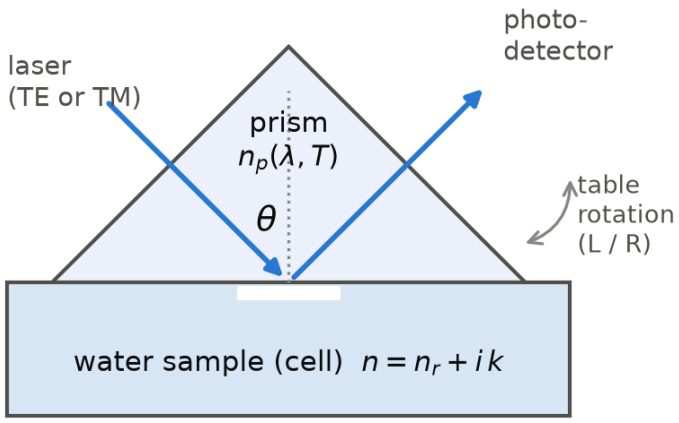


Fig. 1. Geometry of the prism-coupling refractometer. The prism and the water cell rotate together (in direction L or R) relative to the fixed laser and detector; θ is the internal angle of incidence.

4. Data analysis

Each scan is reduced to one derivative-method index, which is then corrected in three steps: rotation-direction averaging, a modelled bias for each polarization, and conversion of the references to the instrument's air scale. All code and intermediate tables are in the `analysis/` folder (Section 8).

Derivative-method index. Isolated one-sample spikes (more than six robust standard deviations from a 5-point running median) are replaced by the median. The intensity is differentiated with a Savitzky–Golay filter (15 points, about 0.054°, quadratic) [22]. The maximum is searched away from the filter's edge samples and refined by a parabola through ±5 points. Then $n_{SDM} = n_p(\lambda, T) \sin \theta_c$. For each scan we also record the full width at half maximum (FWHM) of the derivative peak, its asymmetry and the edge reflectance $R_c = I(\theta_c)/I_{TIR}$, where I_{TIR} is the median intensity 0.3° above θ_c. Two scans that the earlier analysis had mis-located (a spike, and a filter edge artefact) are recovered by these rules; no scan is discarded.

Rotation direction. For each wavelength, temperature and polarization we average L and R scans separately and take $n = (n_L + n_R)/2$, with standard error $\frac{1}{2}(s_L^2 + s_R^2)^{1/2}$. For runs without a direction label the plain mean is used, and its standard error then includes the L/R spread.

Bias model. For each wavelength and temperature we simulate scans from Section 2.2 on a grid of σ (0.004–0.070°) and $\log_{10} k$ (−9 to −3). Each simulated scan goes through the same code as the data, with the measured angular step. The six peak-shape observables (FWHM, asymmetry and R_c for TE and TM) are compared with the measured medians in a χ^2 that includes their standard errors and floors of 0.006°, 0.008° and 0.012. Posterior means over the grid give σ, k and the biases Δ_{TE} and Δ_{TM}. The fit uses only peak shapes, never the indices, so the predicted TE–TM difference has no adjustable parameter. Repeating the inference with a uniform kernel gives a systematic uncertainty for the kernel shape.

Corrected index. $n_{cor} = n - \Delta_{pol}$. Its uncertainty combines the statistical error, the posterior spread of Δ and the kernel-shape term. The anisotropy is $n_{TM} - n_{TE}$ before and after subtracting $\Delta_{TM} - \Delta_{TE}$.

References on the air scale. IAPWS R9-97 gives n relative to vacuum [12, 13]; we evaluate it with the density of air-free water [20] and divide by the index of laboratory air (Ciddor, 25 °C, 101.325 kPa [21]). This lowers the reference by 3.6×10^{-4} at 532 nm and 3.5×10^{-4} at 1551 nm, comparable to the effects studied here. The Kedenburg et al. dispersion formula (20 °C, 0.5–1.6 μm) [14] is moved to 25 °C with the IAPWS temperature coefficient. Extinction coefficients are from Segelstein [15] and Hale & Querry [18].

5. Results

5.1 Reflectance profiles

The profiles have the shape Fresnel theory predicts for an almost transparent sample: a sharp edge at θ_c and a TE curve that lies above the TM curve below it (Fig. 2). At 1551 nm the edge is visibly rounder, and the derivative peak is about twice as wide as at 633 nm (FWHM 0.18° vs 0.085° for TE). In every condition the TE peak is wider than the TM peak and R_c is higher for TE (≈ 0.92 vs ≈ 0.86 at 633 nm).

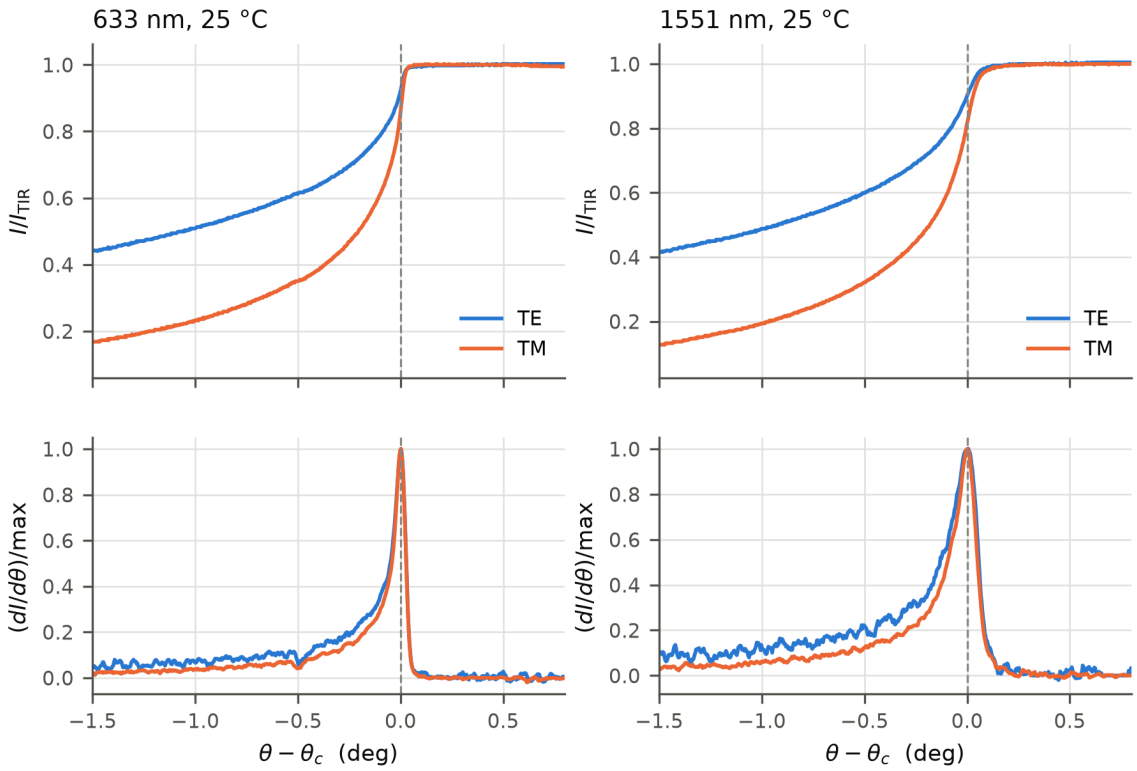


Fig. 2. Normalized intensity (top) and its smoothed derivative (bottom) for one TE and one TM scan at 633 nm and 1551 nm, 25 °C, plotted against the angle from the derivative maximum.

5.2 Rotation direction

Scans taken with the table rotating in direction L read higher than those taken in direction R, by $n_L - n_R = (9.3 \pm 1.8) \times 10^{-4}$ over all 12 condition pairs and $(10.4 \pm 0.6) \times 10^{-4}$ at 25 °C (Fig. 3). The offset is the same for TE and TM, is stable over half an hour of alternating scans, and is 15 times larger than the TE–TM difference. It corresponds to an angular shift of ±0.019° per direction, consistent with a lag between the angle encoder and the detector reading, or with backlash in the drive. Averaging L and R removes it to first order; this was not done in the earlier analysis, which used L scans only.

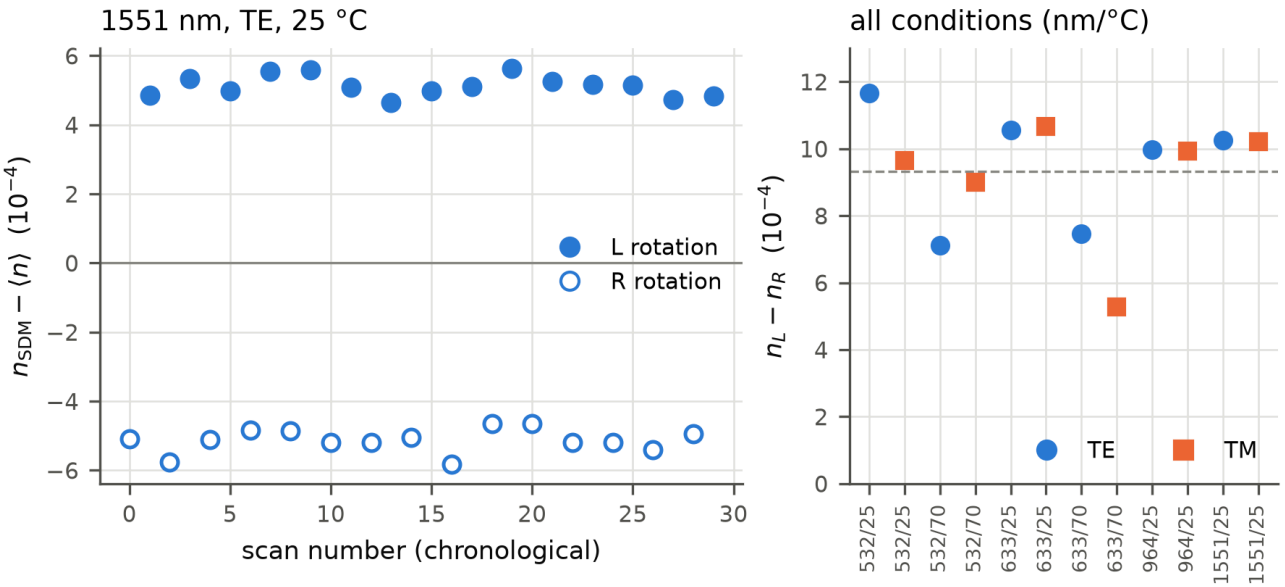


Fig. 3. Left: derivative-method index of 30 consecutive TE scans at 1551 nm, relative to their mean; filled = L, open = R rotation. Right: $n_L - n_R$ for every wavelength/temperature (nm/°C) and polarization; dashed line = mean.

5.3 Bias of the derivative method

The forward model reproduces all six peak-shape observables with χ^2 between 0.6 and 9.8 for 4 degrees of freedom (Table 2). The inferred angular spread is 0.014° at 633 nm, 0.019–0.023° at 532 nm and about 0.025° at 964 and 1551 nm. It is independent of temperature at a given wavelength, as expected for a property of each laser. At 1551 nm the peak shapes also constrain the extinction, $\log_{10} k = -3.6 \pm 1.1$, consistent with the literature value 1.3×10^{-4} [15]. At the other wavelengths k is unconstrained and irrelevant.

With these parameters the derivative method underestimates n by 3.5–6.2 × 10^{-4}, more for TE than for TM (Fig. 4a). The predicted artefact $n_{TM} - n_{TE}$ grows with σ and with k, from +2.9 × 10^{-5} at 633 nm to +8.4 × 10^{-5} at 1551 nm (Fig. 4b). Replacing the Gaussian kernel with a uniform one changes the predicted difference by at most 0.5 × 10^{-5}.

λ (nm)	T (°C)	σ (deg)	χ^2 (4 dof)	Δ_{TE} (10^{-4})	Δ_{TM} (10^{-4})	$\Delta_{TM} - \Delta_{TE}$ (10^{-5})
532	25	0.021 ± 0.002	6.3	−4.66	−4.24	+4.2 ± 0.3
532	50	0.019 ± 0.002	5.2	−4.42	−4.06	+3.7 ± 0.6
532	70	0.020 ± 0.003	2.7	−4.65	−4.22	+4.3 ± 0.3
532	80	0.023 ± 0.003	9.8	−4.98	−4.51	+4.7 ± 0.4
633	25	0.014 ± 0.003	0.6	−3.84	−3.52	+3.2 ± 0.2
633	70	0.014 ± 0.003	0.6	−3.78	−3.49	+2.9 ± 0.5
964	25	0.025 ± 0.004	2.1	−5.26	−4.75	+5.0 ± 0.4
1551	25	0.024 ± 0.008	1.8	−6.18	−5.34	+8.4 ± 0.5

Table 2. Angular spread and derivative-method bias $\Delta = n_{SDM} - n$ inferred from peak shapes. Uncertainties on $\Delta_{TM} - \Delta_{TE}$ include the kernel-shape term.

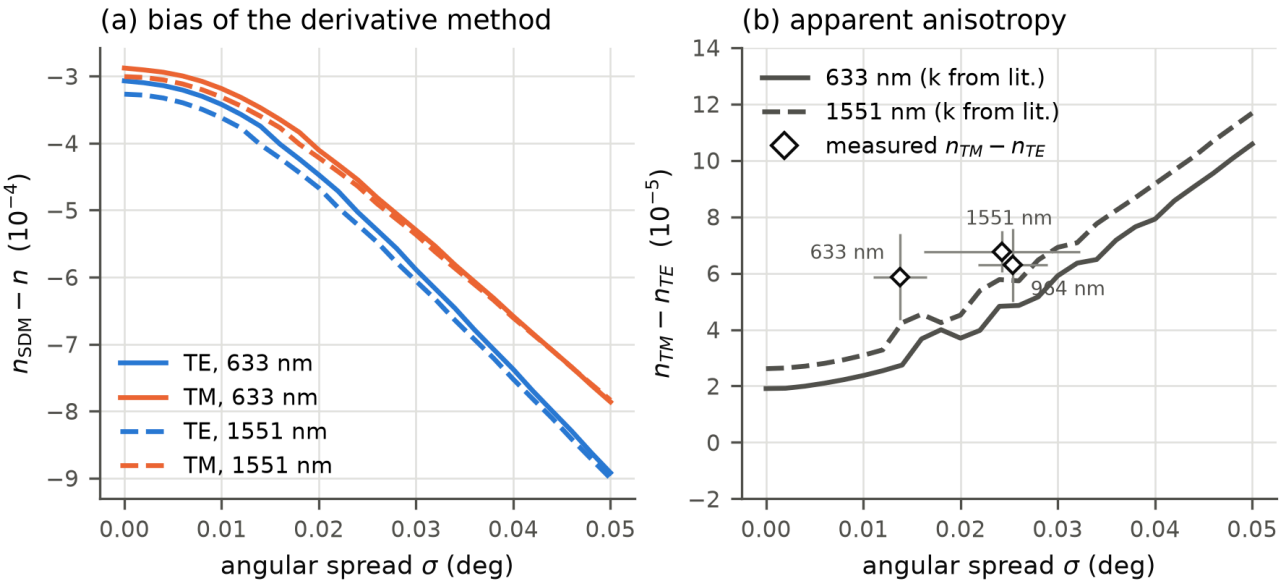


Fig. 4. (a) Simulated bias of the derivative method versus angular spread for TE and TM at 633 and 1551 nm. (b) Predicted apparent anisotropy (lines) and measured $n_{TM} - n_{TE}$ at 25 °C (diamonds) placed at their inferred σ.

5.4 Anisotropy

The derivative method gives $n_{TM} > n_{TE}$ in all six well-measured conditions, with a weighted mean of (6.6 ± 0.6) × 10^{-5} over all eight (Table 3). After subtracting the predicted artefact, the weighted mean is (−0.04 ± 0.65) × 10^{-5} with $\chi^2 = 13.8$ for 7 degrees of freedom (Fig. 5). Scaling the uncertainty by $(\chi^2/\mathrm{dof})^{1/2} = 1.40$ gives (−0.04 ± 0.91) × 10^{-5}, so $|n_{TM} - n_{TE}| < 1.8 \times 10^{-5}$ at 95 % confidence.

The three most precise conditions, all at 25 °C, tell the same story at different wavelengths: the measured gap is +5.9, +6.3 and +6.8 × 10^{-5} at 633, 964 and 1551 nm, and the predicted artefact accounts for all but +2.6 ± 1.5, +1.3 ± 1.4 and −1.6 ± 0.9 × 10^{-5}. The residuals change sign and show no trend with wavelength or with water's absorption, which rises by four orders of magnitude from 633 to 1551 nm.

As a partial check we repeated the analysis with 9- and 21-point smoothing windows. The measured gaps change by up to 2 × 10^{-5}, and the model tracks them to within about 3 × 10^{-5} — consistent with the bound, but not a sharper test.

λ (nm)	T (°C)	Measured $n_{TM} - n_{TE}$	Predicted artefact	Corrected
532	25	+2.4 ± 6.4	+4.2 ± 0.3	−1.8 ± 6.5
532	50	−39 ± 25	+3.7 ± 0.6	−43 ± 25
532	70	+11.3 ± 5.8	+4.3 ± 0.3	+7.0 ± 5.8
532	80	−28 ± 49	+4.7 ± 0.4	−32 ± 49
633	25	+5.9 ± 1.5	+3.2 ± 0.2	+2.6 ± 1.5
633	70	+18 ± 11	+2.9 ± 0.5	+15 ± 11
964	25	+6.3 ± 1.3	+5.0 ± 0.4	+1.3 ± 1.4
1551	25	+6.8 ± 0.7	+8.4 ± 0.5	−1.6 ± 0.9
Weighted mean		**+6.6 ± 0.6**		**−0.04 ± 0.91**

Table 3. TM–TE index difference in units of 10^{-5}. The 50 and 80 °C runs mix rotation directions, hence their large errors.

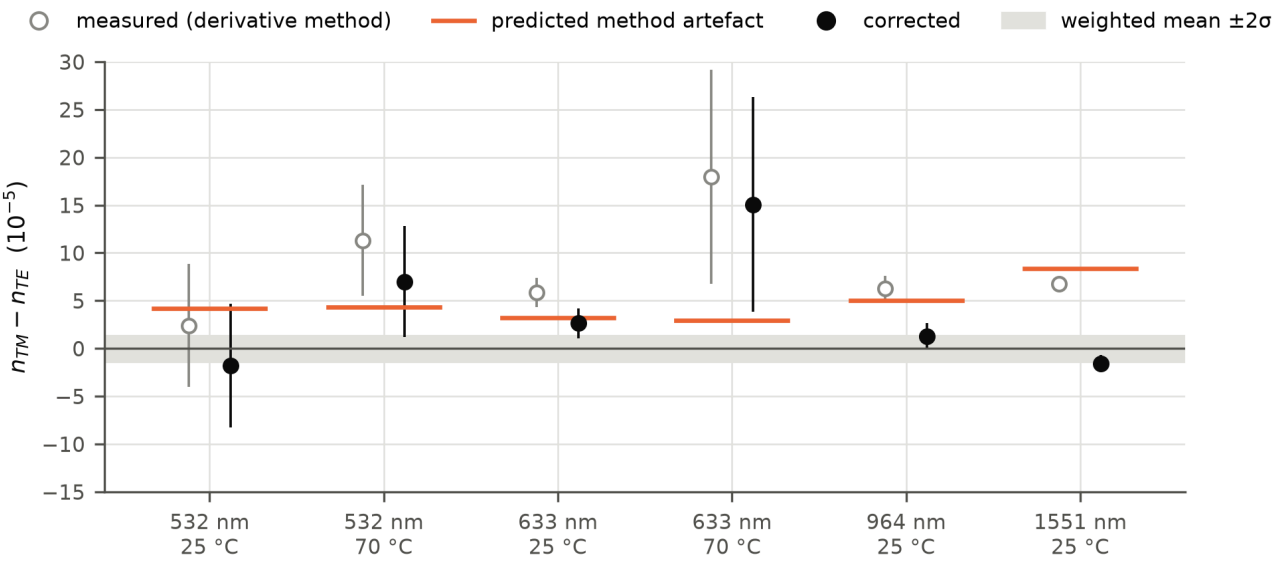


Fig. 5. TM–TE index difference per condition: measured with the derivative method (open), predicted method artefact (bars) and corrected (filled). Grey band: weighted mean ±2σ. The 50 and 80 °C runs (errors > 2 × 10^{-4}) are omitted for clarity.

5.5 Dispersion at 25 °C

The corrected indices agree with IAPWS R9-97 (air scale) to within ±1.0 × 10^{-3} at all four wavelengths, with an rms deviation of 7.4 × 10^{-4} (Table 4, Fig. 6). TE and TM agree to within 3 × 10^{-5} everywhere. The deviations alternate in sign (+5.6, −7.4, −10.1, +5.9 × 10^{-4}) rather than following a smooth curve. That is the signature of a per-session offset from the auto-referencing of each laser (Section 6), not of a dispersion error in the reference.

At 1551 nm, where IAPWS is an extrapolation beyond its validated range, our value 1.31515 lies 5.9 × 10^{-4} above IAPWS and 2.3 × 10^{-4} above the Kedenburg formula moved to 25 °C. Both are within our absolute

uncertainty.

λ (nm)	n_{TE}	n_{TM}	IAPWS (air)	Kedenburg (25 °C)	$n - n_{IAPWS}$ (10^{-4})
532	1.33509	1.33507	1.33453	1.33498	+5.6
633	1.33050	1.33053	1.33126	1.33138	−7.4
964	1.32416	1.32418	1.32517	1.32495	−10.1
1551	1.31516	1.31514	1.31456	1.31492	+5.9

Table 4. Bias-corrected, L/R-averaged indices of water at 25 °C, relative to air. Relative (within-session) uncertainties are 2–8 × 10^{-5}; the absolute uncertainty is ±1 × 10^{-3} (session reproducibility). The last column uses the TE/TM average.

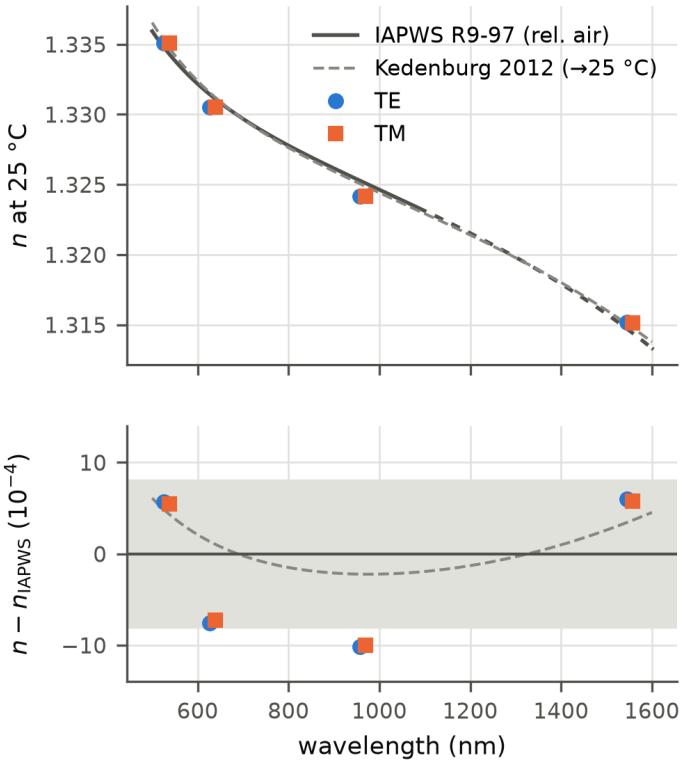


Fig. 6. Top: corrected TE and TM indices at 25 °C with IAPWS R9-97 (solid; broken beyond its 1.1 µm validation limit) and Kedenburg et al. (dashed). Bottom: deviation from IAPWS; grey band = ±8 × 10^{-4} session reproducibility.

5.6 Temperature dependence

At 633 nm, where 70 and 25 °C were measured back to back in one session, the thermo-optic coefficient is (n_{70} − n_{25})/45 K = (−16.04 ± 0.14) × 10^{-5} K^{-1}. IAPWS gives −16.10 × 10^{-5} K^{-1}, a difference of 0.4 % (Fig. 7). The deviation from IAPWS is the same at both temperatures (−7.4 and −7.2 × 10^{-4}), so the offset is constant within a session.

At 532 nm the same calculation gives −19.7 × 10^{-5} K^{-1} against −16.3 × 10^{-5} K^{-1} from IAPWS. However, 25 and 70 °C were measured in different sessions (B and D), with the 633 nm laser used in between. Their offsets from IAPWS (+5.6 and −9.6 × 10^{-4}) differ by 1.5 × 10^{-3}, which accounts for the whole discrepancy. We therefore do not report a 532 nm coefficient.

The 50 and 80 °C runs (session A) scatter by 2–9 × 10^{-4} within a run, against 0.2–1.4 × 10^{-4} per rotation direction at 25 °C. They mix rotation directions, and the 80 °C scans began about 6 min after the 50 °C ones. Their slope at 532 nm, (−15.3 ± 1.0) × 10^{-5} K^{-1} against −20.0 × 10^{-5} K^{-1} from IAPWS, is shown for completeness but is not used.

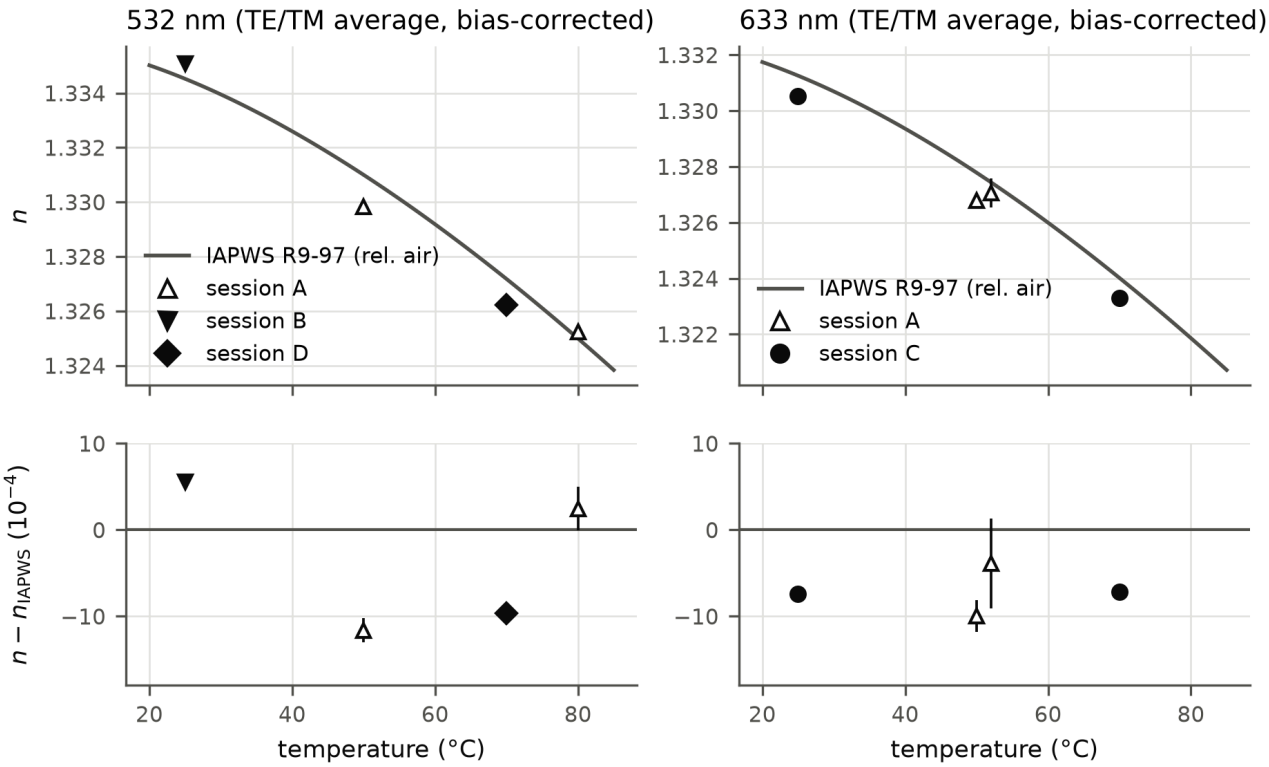


Fig. 7. TE/TM-averaged, bias-corrected index versus temperature at 532 nm (left) and 633 nm (right), with IAPWS R9-97 (air scale). Marker shape = measurement session (Table 1). Bottom: deviation from IAPWS.

6. Discussion and limitations

The anisotropy bound rests on relative measurements made minutes apart with the same prism and laser. The absolute indices rest on the instrument's calibration, which reproduces only to about $\pm 1 \times 10^{-3}$ between sessions.

Session offsets. Within session C the offset from IAPWS at 633 nm is constant to 3×10^{-5} between 25 and 70 °C. Between sessions B and D at 532 nm it jumps by 1.5×10^{-3}. An error of 0.04° in the table's auto-reference gives 1×10^{-3} in n. A change of sample or cell clamping is not the cause: the cell was refilled, re-clamped and re-referenced before every polarization series, yet the corrected TE and TM indices agree to within 3×10^{-5}. With the same laser, refilling and re-referencing therefore reproduce n at that level; the 10^{-3} jumps appear only between sessions in which the laser was changed and realigned. Because TE and TM were measured on separate fillings, a genuine anisotropy and a systematic refill offset cannot be told apart here: the bound applies to their sum, which is consistent with zero at every wavelength. L and R scans alternate within one filling, so the rotation offset cancels.

What the bound covers. The critical angle is set by the semi-infinite medium behind any interfacial layer: for a lossless stack, total reflection begins where the wave becomes evanescent in the bulk, $\sin \theta_c = n_{bulk}/n_p$, whatever thin layers lie in between [19]. A layer much thinner than the wavelength therefore does not move θ_c; it only reshapes the reflectance below θ_c by an amount that scales with d/λ, and moves the derivative maximum far less. The bound thus applies to bulk water, where isotropy is expected by symmetry, and to any ordered layer thick enough ($\gtrsim \lambda$) to act as bulk. Molecular-scale ordering [5–11] lies outside what critical-angle refractometry can detect; ellipsometry or surface-specific spectroscopy is the appropriate tool. In any case the prism surface is a polished high-index crystal or glass (material not recorded), not the hydrophobic surface where the strongest ordering has been reported [8, 10, 11].

Model assumptions. The bias correction assumes a symmetric angular response of fixed shape and Fresnel reflection at a sharp interface. Gaussian and uniform kernels give the same predicted TE–TM difference within

0.5×10^{-5}. The model reproduces six peak-shape observables per condition, with total $\chi^2 = 29$ for 32 degrees of freedom. The residual χ^2 of the corrected anisotropy (13.8 for 7 dof) suggests an extra scatter of about 1×10^{-5}, which we include by scaling the error.

Absorption at 1551 nm. The peak shapes give k = 10^(−3.6 ± 1.1), consistent with the literature 1.3×10^{-4} but too broad to be a measurement. A proper application of the extended derivative method [17] needs absolute reflectance, i.e. an air or reference scan normalized like the turbid-media scans taken later on the same instrument. The water scans have none, and the edge reflectance R_c here is relative to the total-reflection level.

Comparison with the earlier analysis. The 2021 semester report gave $n_{TM} - n_{TE} \approx 5–6 \times 10^{-5}$ from L scans only and called it statistically insignificant. In fact the difference is highly significant (11σ), and it is explained by the derivative method rather than by water.

7. Conclusions

Liquid water at a prism interface shows no polarization dependence of its refractive index: $|n_{TM} - n_{TE}| < 2 \times 10^{-5}$ (95 %) from 532 to 1551 nm.

1. The standard derivative method makes an isotropic liquid look birefringent. For water it returns $n_{TM} - n_{TE} = +3$ to $+8 \times 10^{-5}$, because the instrument's angular spread and the sample's absorption shift the TE and TM derivative maxima by different amounts.
2. That artefact can be predicted from the measured peak shapes alone, with no parameter fitted to the indices, and removed.
3. The rotation direction of the table shifts n by $\pm 5 \times 10^{-4}$; alternating directions and averaging removes it.
4. After these corrections the indices agree with IAPWS R9-97 (converted to the air scale) within the $\pm 1 \times 10^{-3}$ session reproducibility, including at 1551 nm. The 633 nm thermo-optic coefficient, -16.04×10^{-5} K^{-1}, matches IAPWS to 0.4 %.

In practice: for TE and TM light alike, IAPWS R9-97 divided by the index of air is a good approximation for n of water on a prism-coupler scale between 532 and 1551 nm and 25–70 °C. Any polarization dependence below 2×10^{-5} has yet to be found. Future measurements should alternate polarization and rotation direction within one filling and one calibration, record an air reference for the extended derivative method, and step temperature only after the reading has settled.

8. Data, code and credit

A representative sample of the raw scans is provided with this release for verification (`data_sample/`, 16 files: water at 964 and 1551 nm in both polarizations and rotation directions, Intralipid at 1551 nm and cream at 633 nm with their air references). The full dataset (252 water scans, and 115 Intralipid and cream scans with their air references) was recorded at EDML, UNIWA; it may be the property of the laboratory and is not disclosed. The complete analysis code is included (`code/`): it reproduces every number in this paper when run on the full dataset, and processes the sample files individually.

Measurements: Ierotheos Katsoulis, Electronic Devices and Materials Laboratory (EDML), University of West Attica, during an MSc by Research supervised by Prof. Konstantinos Moutzouris. Analysis and text: Ierotheos Katsoulis, 2026.

References

1. S. Singh, "Refractive index measurement and its applications," Phys. Scr. 65, 167–180 (2002). doi:10.1238/Physica.Regular.065a00167

2. R. Th. Kersten, "A new method for measuring refractive index and thickness of liquid and deposited solid thin films," Opt. Commun. 13, 327–329 (1975). doi:10.1016/0030-4018(75)90112-1
3. G. H. Meeten, "Refractive index errors in the critical-angle and the Brewster-angle methods applied to absorbing and heterogeneous materials," Meas. Sci. Technol. 8, 728–733 (1997). doi:10.1088/0957-0233/8/7/006
4. I. Thormählen, J. Straub, U. Grigull, "Refractive index of water and its dependence on wavelength, temperature, and density," J. Phys. Chem. Ref. Data 14, 933–945 (1985). doi:10.1063/1.555743
5. M. Maccarini, "Water at solid surfaces: a review of selected theoretical aspects and experiments on the subject," Biointerphases 2, MR1–MR15 (2007). doi:10.1116/1.2768902
6. D. O. Shah, R. M. Hamlin, "Structure of water in microemulsions: electrical, birefringence, and nuclear magnetic resonance studies," Science 171, 483–485 (1971). doi:10.1126/science.171.3970.483
7. S. Dietrich, "Structures in fluids induced by interfaces," J. Phys.: Condens. Matter 8, 9127–9141 (1996). doi:10.1088/0953-8984/8/47/004
8. V. M. Gun'ko et al., "Unusual properties of water at hydrophilic/hydrophobic interfaces," Adv. Colloid Interface Sci. 118, 125–172 (2005). doi:10.1016/j.cis.2005.07.003
9. P. D. Spencer, J. D. Riches, E. D. Williams, "Exclusion zone water is associated with material that exhibits proton diffusion but not birefringent properties," Fluid Phase Equilib. 466, 103–109 (2018). doi:10.1016/j.fluid.2018.03.020
10. S. Strazdaite, J. Versluis, E. H. G. Backus, H. J. Bakker, "Enhanced ordering of water at hydrophobic surfaces," J. Chem. Phys. 140, 054711 (2014). doi:10.1063/1.4863558
11. S. Strazdaite, J. Versluis, H. J. Bakker, "Water orientation at hydrophobic interfaces," J. Chem. Phys. 143, 084708 (2015). doi:10.1063/1.4929905
12. IAPWS R9-97, "Release on the refractive index of ordinary water substance as a function of wavelength, temperature and pressure" (1997). iapws.org
13. A. H. Harvey, J. S. Gallagher, J. M. H. Levelt Sengers, "Revised formulation for the refractive index of water and steam as a function of wavelength, temperature and density," J. Phys. Chem. Ref. Data 27, 761–774 (1998). doi:10.1063/1.556029
14. S. Kedenburg, M. Vieweg, T. Gissibl, H. Giessen, "Linear refractive index and absorption measurements of nonlinear optical liquids in the visible and near-infrared spectral region," Opt. Mater. Express 2, 1588–1611 (2012). doi:10.1364/OME.2.001588 (formula)
15. D. J. Segelstein, "The complex refractive index of water," M.S. thesis, University of Missouri–Kansas City (1981).
16. T.-Q. Sun et al., "Scanning focused refractive-index microscopy," Sci. Rep. 4, 5647 (2014). doi:10.1038/srep05647
17. S. Koutsoumpos, P. Giannios, I. Stavrakas, K. Moutzouris, "The derivative method of critical-angle refractometry for attenuating media," J. Opt. 22, 075601 (2020). doi:10.1088/2040-8986/ab8286
18. G. M. Hale, M. R. Querry, "Optical constants of water in the 200-nm to 200-µm wavelength region," Appl. Opt. 12, 555–563 (1973). doi:10.1364/AO.12.000555 (data)
19. M. Born, E. Wolf, Principles of Optics, 7th ed. (Cambridge University Press, 1999).
20. G. S. Kell, "Density, thermal expansivity, and compressibility of liquid water from 0° to 150°C," J. Chem. Eng. Data 20, 97–105 (1975). doi:10.1021/je60064a005
21. P. E. Ciddor, "Refractive index of air: new equations for the visible and near infrared," Appl. Opt. 35, 1566–1573 (1996). doi:10.1364/AO.35.001566
22. A. Savitzky, M. J. E. Golay, "Smoothing and differentiation of data by simplified least squares procedures," Anal. Chem. 36, 1627–1639 (1964). doi:10.1021/ac60214a047
23. Metricon Corporation, Model 2010/M prism coupler. metricon.com